

SUPPLEMENTARY MATERIAL

Active faulting controls bedform development on a deep-water fan

Authors

Vittorio Maselli¹, Aaron Micallef^{2,3}, Alexandre Normandeau⁴, Davide Oppo⁵, David Iacopini⁶, Andrew Green⁷, Zhiyuan Ge⁸

Affiliations

¹ Department of Earth and Environmental Sciences, Dalhousie University, Halifax, Nova Scotia, B3H 4R2, Canada

² Marine Geology and Seafloor Surveying, Department of Geosciences, University of Malta, Msida 1805, Malta

³ Helmholtz Centre for Ocean Research, GEOMAR, 24148 Kiel, Germany

⁴ Geological Survey of Canada, Natural Resources Canada, Dartmouth, Nova Scotia, B2Y 4A2, Canada

⁵ School of Geosciences, University of Louisiana at Lafayette, Lafayette, Louisiana 70504, USA

⁶ DiSTAR (Department of Earth, Environmental and Resources Sciences), Università di Napoli Federico II, 80138 Naples, Italy

⁷ Geological Sciences, University of KwaZulu-Natal, Durban 4041, South Africa

⁸ College of Geosciences, China University of Petroleum, Beijing 94305, China

S1 - Numerical modelling.

The approach involved for turbidity current modelling is largely similar to previous numerical studies on turbidity current responses to various topographic settings, where the simulations are performed on the Flow3D platform (e.g., Ge et al., 2017; Howlett et al., 2019). In detail, the numerical model presented in this study deploys Reynolds-Averaged Navier-Stokes (RANS) equations with Renormalization Group (RNG) $k - \varepsilon$ model to describe the fluid motion in turbidity current. The bedload sediment is modelled with Meyer-Peter and Muller (1948) formula and the sediment entrainment is solved using Mastbergen and Van Den Berg (2003) formula.

The key parameters of the turbidity current used in the simulation is similar to the study of Covault et al. (2014) where the supercritical turbidity current form depositional cyclic steps. In the simulation, a uniform sediment-water mixture was released from the inlet towards the downslope on the simplified topography for 2 hours with an initial velocity of 1.5 m/s. The inlet is 15 m in height and 800 m in width. The fault scarp is located 12 km away from the inlet (Fig. 4 in the paper). The topography has no lateral variations, but the model was designed to have same

width as the inlet to account for 3-D variations within the flow. The grid resolution is chosen to be different in three dimensions in order to accommodate the simulation in the workstation without compromising its physical reality (Table 1). The simulation stops at 2 hours and 25 minutes as the flow head leaves the simulation domain.

Once the flow left the inlet, it collapsed to roughly 10 m thick at c. 200 m away from the inlet before growing thicker to a few tens of meters as the ambient water entrained in the flow. Along with collapsing of the flow, the turbidity current also accelerated to over 2 m/s and more or less maintained such velocity until crossing over the fault escarpment where it dropped to blow 2 m/s (Fig. 4 in the paper). As water entrained in the upper part of the flow, more and more sediment concentrated in the bottom part increasing the sediment volume concentration to over 0.6% at 4 km away from the inlet.

Table 1: Cell sizes of the grid along different directions

X	Y	Z
17m	8-53 m	1.25-2.5 m

S2 - Bathymetric profiles along the thalwegs of the canyons.

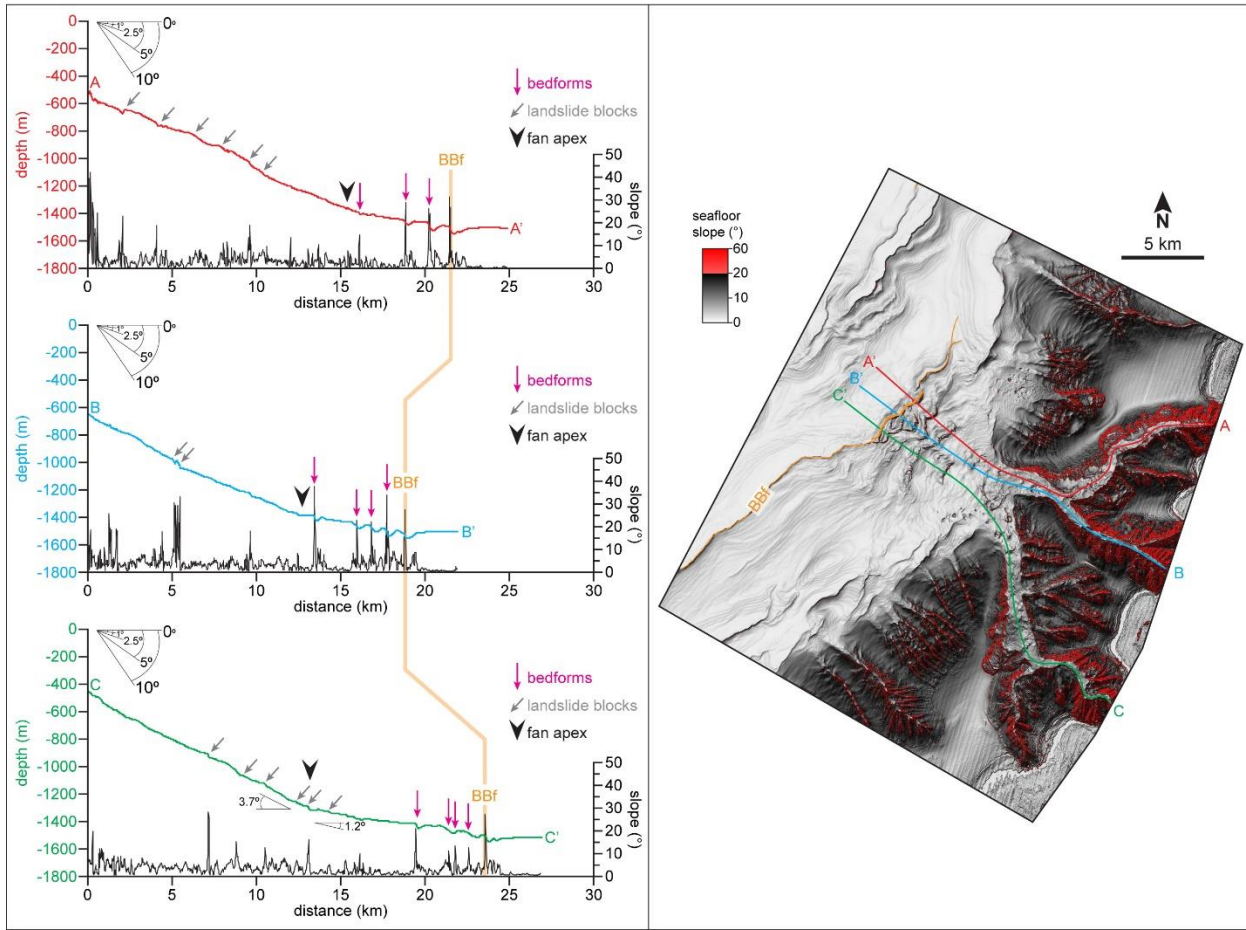


Figure 1. Left: Bathymetric profiles along the thalwegs of the three canyons and corresponding seafloor slope gradients (see map on the right for location). Orange line: Bedform Bounding fault (BBf). Right: seafloor slope map with location of the bathymetric sections (violet, blue, and green lines) and the BBf (orange).

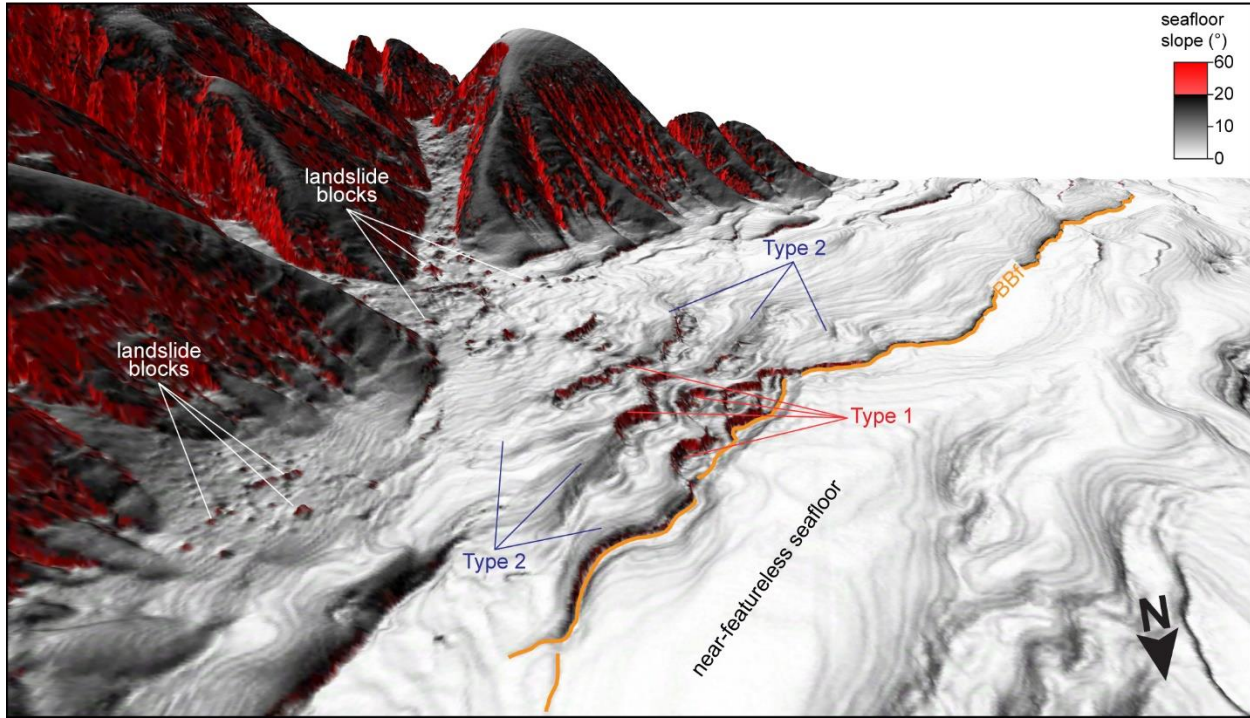
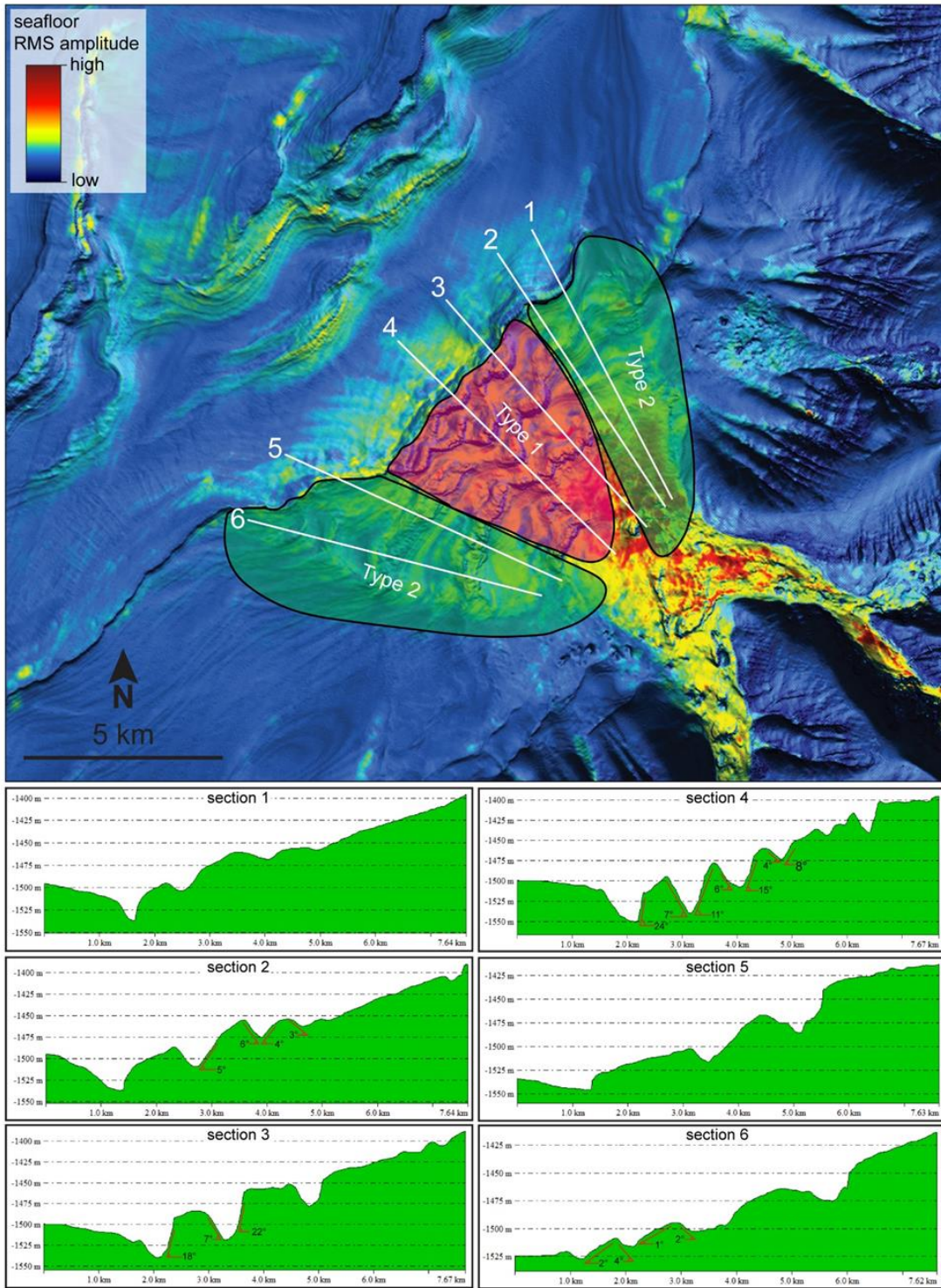


Figure 2. 3-D view of the seafloor with slope gradient. Notice how the Bedform Bounding fault (BBf, orange line) is partially reworked by type 1 bedforms on the fan. Landslide blocks along the canyons are also highlighted.

S3 - Bathymetric profiles across type 1 and type 2 bedforms.



S4 - 3-D view of the study area.

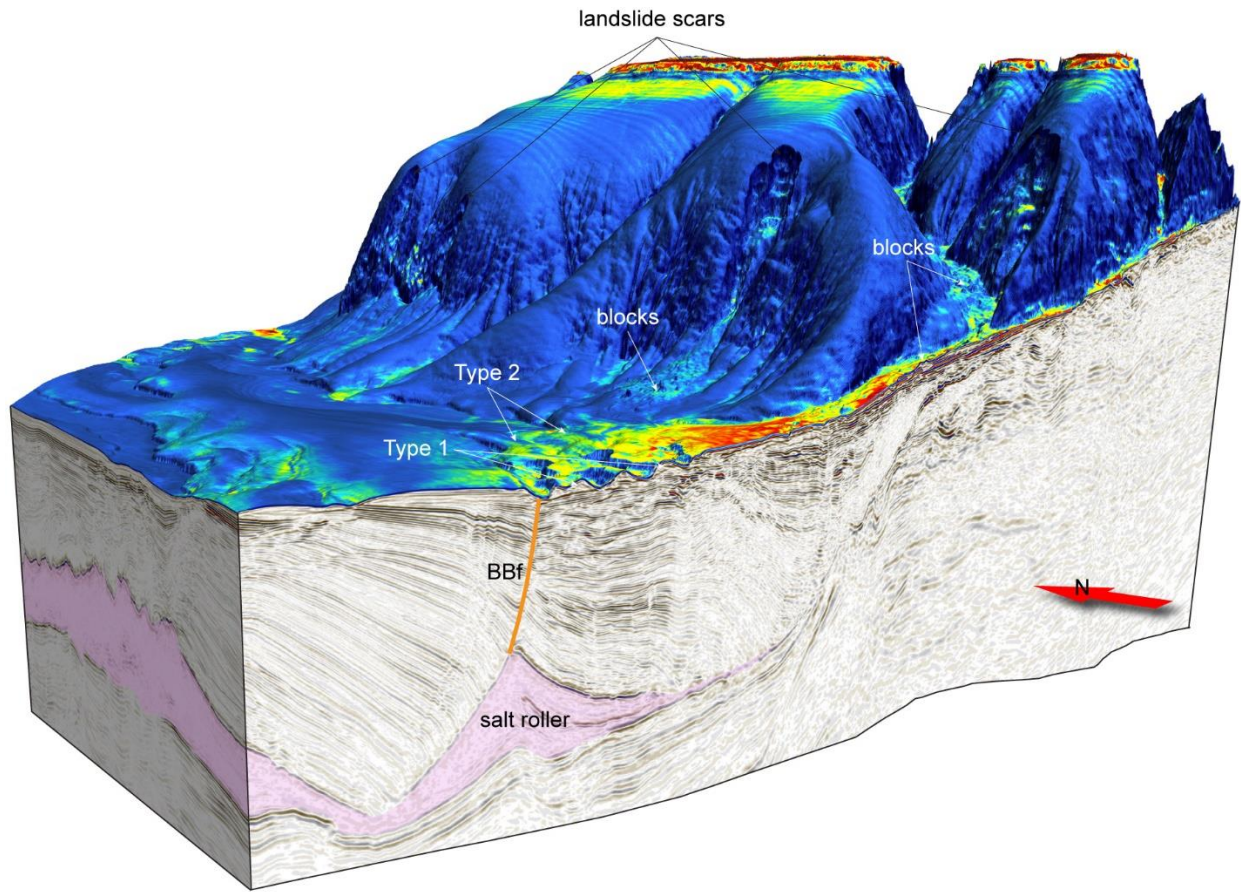


Figure 4. 3-D view of the seafloor with RMS amplitude attribute. The seismic section facing to the south is extracted along the thalweg of the southernmost canyon. Salt deposits are in pink. Orange line is the Bedform Bounding fault (BBf).

S5 - Seafloor bathymetry and thickness map of post-salt deposits.

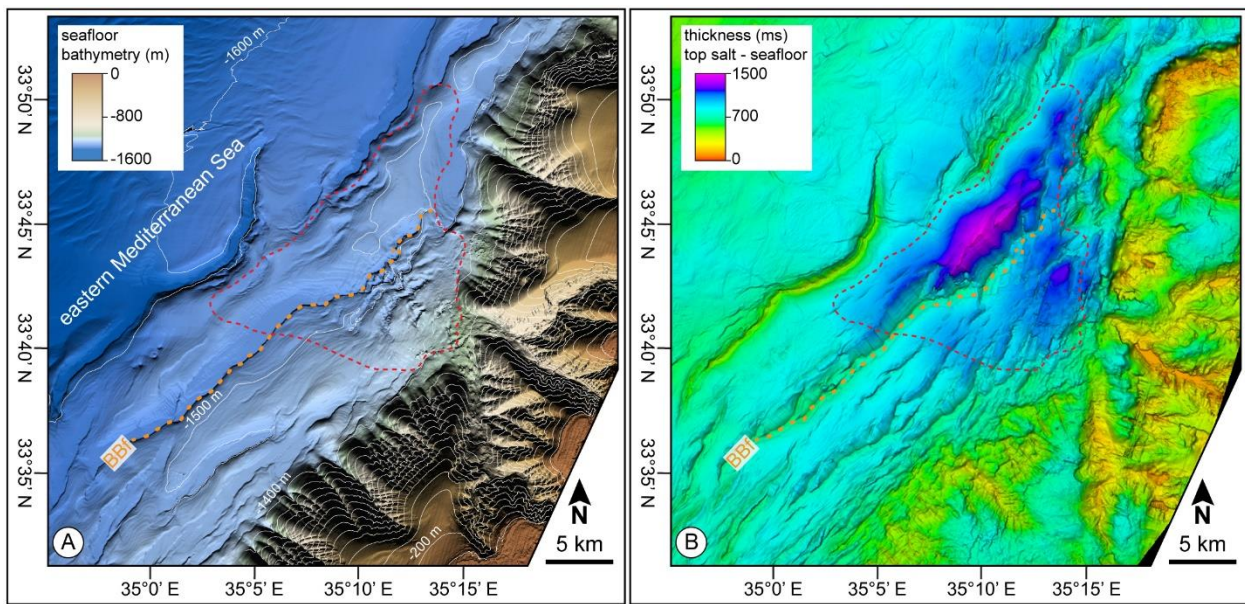


Figure 5. (A) Bathymetry of the seafloor with location of the deep-water fan investigated in this study (red dashed line) and the Bedform Bounding fault (BBf, orange dashed line). (B) Thickness distribution, in milliseconds (ms), of the deposits confined between the top-salt horizon and the seafloor. Note the location of the deep-water fan, confined by a red dashed line.

S6 - New sediment waves seaward of the fan.

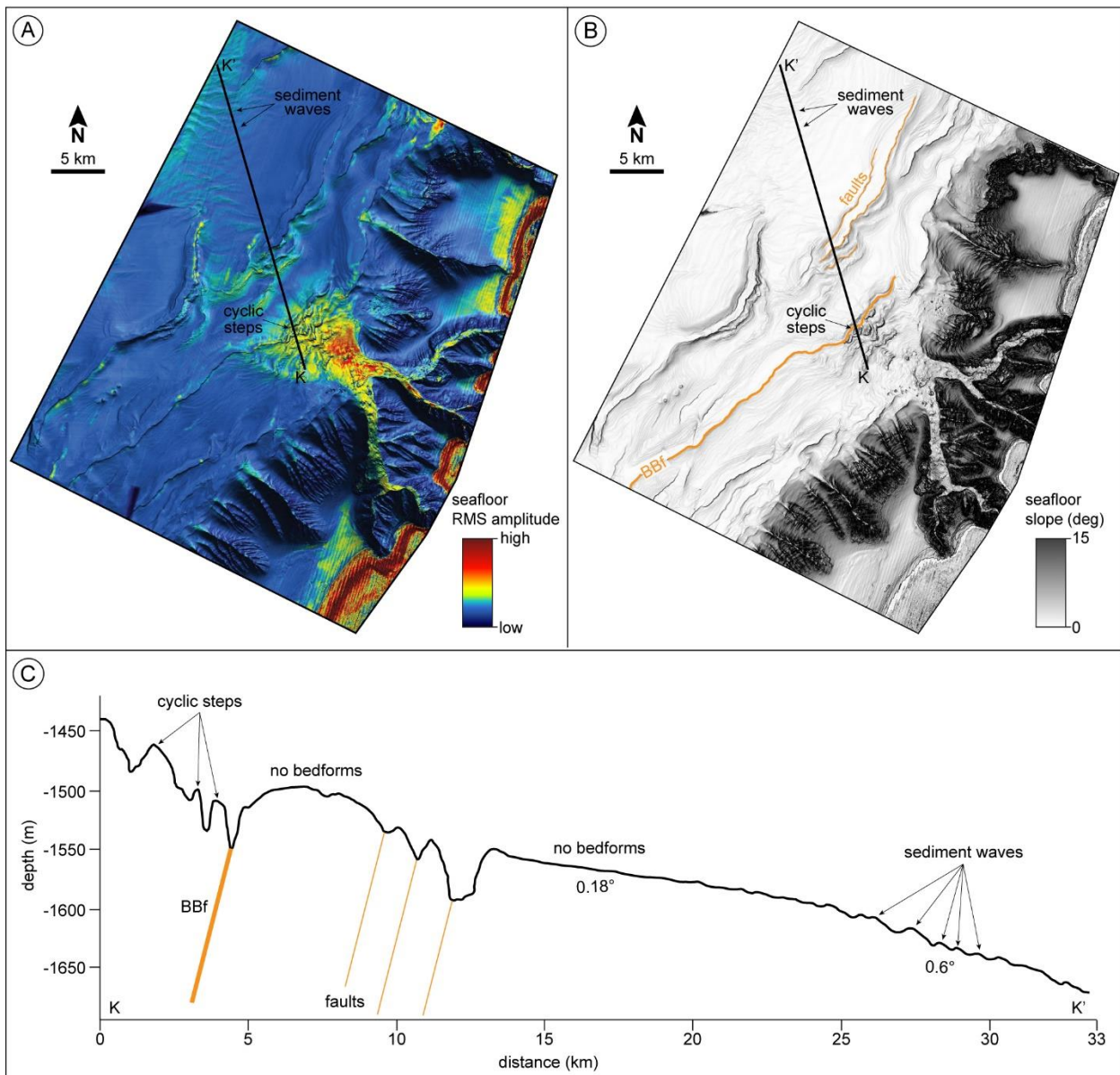


Figure 6. (A) Seafloor map with root-mean-square (RMS) amplitude attribute. (B) Seafloor map with slope gradient. Fault escarpments are in orange and the Bedform Bounding fault (BBf) is marked by a thicker line. Black line is the bathymetric profile (K-K') presented in C. (C) Bathymetric profile K-K', note that new sediment waves with km-scale wavelength develop where there is an increase in seafloor slope from 0.18° to 0.6° .

References

Covault, J.A., Kostic, S., Paull, C.K., Ryan, H.F., Fildani, A., 2014, Submarine channel initiation, filling and maintenance from sea-floor geomorphology and morphodynamic modelling of cyclic steps: *Sedimentology*, v. 61, p. 1031–1054.

Ge, Z., Nemec, W., Gawthorpe, R.L., Hansen, E.W.M., 2017, Response of unconfined turbidity current to normal-fault topography: *Sedimentology*, v. 64, p. 932–959.

Howlett, D.M., Ge, Z., Nemec, W., Gawthorpe, R.L., Rotevan, A., Jackson, C.A.-L., 2019, Response of unconfined turbidity current to deep-water fold and thrust belt topography: Orthogonal incidence on solitary and segmented folds: *Sedimentology*, v. 66, p. 2425–2454.

Mastbergen, D.R., Van den Berg, J.H., 2003, Breaching in fine sand and the generation of sustained turbidity currents in submarine canyons: *Sedimentology*, v. 50, p. 625–637.

Meyer-Peter, E., Muller, R., 1948, Formulas for bed-load transport. Proc. of the 2nd Meeting of IAHSR., Appendix 2. Stockholm, v. 3, p. 39–64.